metals

MDPI

Article

Correlation Between the Accelerated-Rate Decay Mechanism in Neutral Salt Spray Tests and the Atmospheric Corrosion Kinetics Model of a 7075 Aluminum Alloy in Marine Environments

Changjing Cui [1], Xianlian Mu [2], Zuodong Sun [2] and Kui Xiao [3,*]

[1] Beijing Aeronautical Research Center of Engineering & Technology, Beijing 100076, China; cuichangjing@163.com
[2] Key Laboratory of Corrosion Protection and Control of Aviation Technology, China Special Vehicle Research Institute, Jingmen 448035, China; muxl@avic.com (X.M.); sunzuodong2000@163.com (Z.S.)
[3] Institute for Advanced Materials and Technology, University of Science and Technology Beijing, Beijing 100083, China
* Correspondence: xiaokui@ustb.edu.cn

Abstract

This study established a marine atmospheric corrosion prediction model by comparing the corrosion behavior of 7075 aluminum alloy in neutral salt spray tests and outdoor exposure tests conducted in the coastal atmosphere of Hainan. The results show that severe rusting occurred after 96 h of neutral salt spray testing, with loose white cluster-like corrosion products mainly composed of $Al(OH)_3$ and Al_2O_3. The thickening of the corrosion product layer slowed down the corrosion process, following a nonlinear power-law kinetic relationship. In the later stage, potential dropped sharply due to product layer spallation, and recovered as new corrosion products formed, confirming that the stability of the product layer is critical for protection. Under coastal atmospheric exposure, the composition of corrosion products was similar to that observed in the salt spray test, but the actual corrosion rate was affected by environmental dynamic equilibrium. The acceleration factor of the neutral salt spray test corresponding to the same corrosion amount in the Hainan marine atmosphere exhibited a declining trend, reflecting that differences in the protective nature of the corrosion product layer were influenced by environmental factors. Electrochemical analysis indicated that both tests showed similar current–potential synergistic variation mechanisms dominated by product layer stability. In summary, while the neutral salt spray test effectively simulates the chloride-induced corrosion mechanism in marine atmospheres, its kinetic model cannot directly predict real corrosion behavior through a simple acceleration factor, as environmental complexity must be considered.

Keywords: 7075 aluminum alloy; neutral salt spray test; marine atmospheric environment; correlation; acceleration factor

Check for updates

Academic Editor: Eric Hug

Received: 25 November 2025
Revised: 19 December 2025
Accepted: 23 December 2025
Published: 29 December 2025

Copyright: © 2025 by the authors. Licensee MDPI, Basel, Switzerland. This article is an open access article distributed under the terms and conditions of the Creative Commons Attribution (CC BY) license.

1. Introduction

Pure aluminum exhibits excellent corrosion resistance, and its abundance in the Earth's crust along with a simple extraction process gives it a cost advantage over other common metals. However, the relatively low strength of pure aluminum limits its application in certain fields despite its good corrosion resistance [1,2]. Aluminum alloys are produced by alloying pure aluminum with other elements to achieve superior mechanical and functional properties. Due to variations in the type and amounts of alloying elements, different

series of aluminum alloys exhibit distinct performance characteristics suitable for diverse applications. Consequently, the type and content of alloying elements directly influence key properties such as the corrosion resistance of aluminum alloys [3,4].

For instance, 7xxx series aluminum alloys (typical grade 7075, mainly composed of Al–Zn–Mg–Cu) are widely used in aircraft manufacturing for critical load-bearing components such as fuselage frames, wing spars, and stringers, owing to their excellent specific strength, toughness, stiffness-to-weight ratio, and superior machinability and weldability [5]. However, in chloride-rich marine atmospheric environments, these alloys are highly susceptible to localized corrosion, particularly pitting, intergranular corrosion, and stress corrosion cracking [6].

The corrosion failure of aluminum alloys is closely related to environmental factors. Marine atmospheric environments are characterized by high relative humidity, elevated temperature, and high salt content. In such environments, seawater vapor readily condenses and evaporates on metal surfaces, leading to the deposition of salt particles [7]. Therefore, temperature, humidity, chloride ion concentration in seawater, and ultraviolet radiation are key factors influencing the corrosion resistance of aluminum alloys [8,9].

Long-term outdoor exposure studies have demonstrated that the exfoliation corrosion of aluminum alloys in tropical atmospheric environments is primarily caused by the combined effects of hydrogen-assisted intergranular cracking and the volumetric expansion of corrosion products [10]. Analyses of surface morphology, weight loss, and electrochemical data have shown that the corrosion type of aluminum alloys evolves over time, typically progressing from pitting to intergranular corrosion and eventually to exfoliation corrosion [11].

Outdoor stress corrosion tests on 6xxx series aluminum alloys under marine atmospheric exposure indicate that pitting is the dominant corrosion feature, with corrosion products generally exhibiting polygonal morphology [12,13]. Similar exposure tests on 7xxx series aluminum alloys revealed the formation of dense oxide layers, where the corrosion product film typically displays a sandwich-like structure (Al_2O_3/hydroxy chlorinated aluminum/$Al(OH)_3$) [14–16]. The limited increase in corrosion products over time suggests that the dense oxide layer formed under hot and humid marine atmospheric conditions provides effective protection to the underlying alloy substrate.

Investigations on aluminum alloys exposed in coastal environments further show that different alloy compositions lead to distinct corrosion behaviors. For instance, 2xxx and 5xxx series alloys both exhibit pronounced pitting corrosion, with corrosion products mainly composed of Al_2O_3 and AlO(OH), while the latter generally shows better corrosion resistance under the same conditions [17–20].

Although outdoor exposure tests of aluminum alloys can realistically reflect the corrosion behavior and mechanisms in actual service environments, their complexity and long duration make them insufficient to meet the growing demand for research efficiency and product development capacity. Consequently, the research focus of aluminum alloy corrosion evaluation has gradually shifted from outdoor exposure tests to indoor accelerated tests [21–23].

Among these, the salt spray accelerated test can effectively simulate the corrosion mechanism of chloride ions in marine atmospheric environments by establishing a quantitative relationship between chloride concentration and aluminum alloy corrosion rate [24,25]. However, traditional neutral salt spray tests tend to overlook the coupling effects of environmental parameters, leading to prediction deviations. Recent studies have improved model accuracy by quantifying the synergistic effects of key factors, further expanding real-time monitoring approaches for corrosion evaluation. One study employed electrical resistance sensors to monitor the real-time corrosion of $Al_{94}Cu_6$ and 2024-T3 aluminum

alloys under chloride-contaminated atmospheres, revealing that corrosion rates peaked at 70–80% RH during wet–dry transitions and that the ER method provided reproducible, surface-averaged data useful for developing more representative accelerated corrosion tests [26]. A time-of-wetness dominated model further demonstrated that humidity accumulation contributes more than 60% to the overall corrosion process, highlighting its controlling influence [27]. At present, salt spray testing remains a commonly employed standard evaluation method in engineering practice. However, aluminum alloys operating in marine environments face uncertainties and inaccuracies in acceleration factors, with distinct variations in the salt spray acceleration patterns observed across different aluminum alloys. Consequently, the correlation between salt spray testing and marine atmospheric conditions remains unclear [28].

In this study, the corrosion behavior of 7075 aluminum alloy was investigated through neutral salt spray tests. By analyzing the correlations between the corrosion kinetics, corrosion product composition, and electrochemical mechanisms obtained from both the neutral salt spray tests and outdoor exposure tests conducted in the coastal atmosphere of Hainan, a reasonable acceleration factor for the neutral salt spray test was determined. Based on these results, a corrosion prediction model for 7075 aluminum alloy in marine atmospheric environments was established.

This study systematically compares the corrosion kinetics, product composition, and electrochemical mechanisms of 7075 aluminum alloy in neutral salt spray tests and long-term outdoor exposure tests in Hainan's marine atmosphere. It elucidates the intrinsic relationship between accelerated corrosion in controlled environments and natural marine atmospheric corrosion from multiple dimensions. Secondly, a dynamic acceleration factor model decreasing with exposure duration is established, overcoming the limitations of traditional studies employing fixed acceleration factors for corrosion prediction and enhancing the accuracy of marine atmospheric corrosion assessment. Finally, the study reveals that the stability of the corrosion product layer governs the synergistic current-potential variation mechanism in both test environments. This provides a theoretical basis for optimizing accelerated corrosion testing methods for 7xxx series aluminum alloys and guides the precise prediction of their service life in marine environments.

2. Experimental Methods

2.1. Material

The 7075 aluminum alloy plates were selected as the research material. The plates had a thickness of 2.0 mm and were cut into specimens with dimensions of 100 × 50 × 2 mm. Prior to testing, the specimens were ground with sandpaper up to 1500 grit. After polishing, the length, width, and thickness of each specimen were measured three times using a vernier caliper, and the mass was recorded with an electronic balance having a precision of 0.0001 g. Specimens with dimensions of 10 × 10 × 2 mm were prepared for SEM, EDS, and XRD analyses. The chemical composition of the 7075 aluminum alloy used in the experiments is shown in Table 1.

Table 1. Chemical composition of the aluminum alloy (%, by mass).

Si	Fe	Cu	Mn	Mg	Cr	Zn	Al
0.4	0.5	2	0.3	2.9	0.28	6.1	87.32

2.2. Methods

2.2.1. Neutral Salt Spray Test

The neutral salt spray test was conducted using a Q-FOG salt spray accelerated testing chamber. A 5% NaCl solution was used as the salt spray medium, and the test durations were set at 96 h, 240 h, 480 h, 720 h, and 1008 h. For each exposure period, six specimens were taken. The first three specimens were descaled according to the GB/T 16545-2015 standard [29] "Corrosion of metals and alloys—Removal of corrosion products from corrosion test specimens". Nitric acid was used as the descaling solution, and the specimens were immersed in an ultrasonic cleaner at room temperature for 4 min. After descaling, the specimens were rinsed with deionized water, dehydrated with 100% ethanol, dried with air, and weighed.

2.2.2. Outdoor Exposure Test

The outdoor exposure test was conducted in Wenchang, Hainan Province, which represents a typical marine atmospheric environment. Wenchang is located at 110.8° E and 19.6° N, in a coastal inland region characterized by high temperature and humidity throughout the year. According to regional climate data, the annual average rainfall is approximately 1975 mm, with an average temperature of 24.1 °C and a relative humidity of about 86%. Due to the high chloride content in marine environments, Cl^--related parameters were included in the environmental spectrum design. The airborne chloride concentration in Wenchang ranges from 0.056 to 0.225 mg/m^3, and the average chloride deposition rate reaches approximately 54 mg·m^{-2}·d^{-1}.

The outdoor exposure tests were performed in accordance with the GB/T 14165-2008 standard [30]. The aluminum alloy specimens were mounted on racks with the front side facing upward at a 45° angle to the ground. The exposure began in April 2024, and sampling and characterization were carried out after 6 months, 12 months, and 21 months of exposure. For each exposure period, five parallel specimens were used: one for electrochemical testing, one for corrosion product morphology and composition analysis, and the remaining three for surface morphology and kinetic analysis after rust removal according to the standard procedure. The weight loss data obtained after descaling were collected throughout the test for model validation.

2.2.3. Corrosion Morphology Characterization

After each sampling period in both the outdoor exposure and indoor accelerated tests, the macroscopic surface morphology of the 7075 aluminum alloy specimens before and after testing was recorded using a Nikon D7000 digital camera (Nikon Corporation, Tokyo, Japan). The purpose of this observation was to visually document the surface changes occurring during the corrosion process.

Following each sampling period, a KEYENCE VK-X250 3D laser confocal microscope (Keyence Corporation, Osaka, Japan) was employed to examine the microscopic morphology and measure the corrosion depth. The microscopic images were also used for subsequent machine learning–based image analysis, while the depth data were utilized to quantify the corrosion rate. In addition, an FEI Quanta 250 environmental scanning electron microscope (ESEM) (Oxford Instruments, Oxford, UK) was used to observe and analyze both the surface and cross-sectional morphologies of the corroded specimens.

2.2.4. Methods for Analysing Corrosion Products

The chemical composition of the corrosion products was analyzed using energy-dispersive X-ray spectroscopy (EDS) and X-ray diffraction (XRD). EDS was employed to

determine the elemental types and contents in localized microregions of the material, while XRD was used for structural and phase identification of the corrosion products.

Since most aluminum alloys generate only a small amount of corrosion products that cannot be easily collected or ground into powder, the corroded specimens were cut into 10 × 10 mm samples for direct surface analysis. XRD measurements were performed using a Bruker D8 ADVANCE rotating anode diffractometer (Brook Dalton Company, Billerica, MA, USA) equipped with a Co target. The scanning range was set from 10° to 90°, with a scanning rate of 6°/min.

2.2.5. Corrosion Kinetics Analysis

For aluminum alloys, significant weight changes can be observed after both neutral salt spray tests and outdoor exposure tests. Therefore, the weight loss method was employed to calculate the corrosion mass loss and corrosion rate. After standard rust removal, the specimens were weighed to obtain the mass loss data.

The aluminum alloy specimens were weighed before testing and again after rust removal at the end of each test period, and their dimensions were recorded prior to testing. Based on the weight difference before and after corrosion, the average mass loss per unit area and the corresponding corrosion rate at different stages were calculated using the following equations:

$$\Delta W = (W_0 - W_t)/S \quad (1)$$

$$V = \Delta W/t \quad (2)$$

where ΔW is the corrosion mass loss per unit area ($g \cdot m^{-2}$), W_0 and W_t represent the specimen weights before and after rust removal (g), respectively, S is the exposed surface area of the specimen (m^2), and t is the exposure time (h).

In general, the relationship between metal weight loss and exposure time follows a nonlinear power-law kinetic equation expressed as follow:

$$\Delta W = At^n \quad (3)$$

where A and n are constants. The parameter A represents the initial corrosion rate of the aluminum alloy, with a higher A value indicating a faster initial corrosion rate. The parameter n characterizes the protective behavior of the corrosion product layer and its subsequent interaction with the environment; a smaller n value suggests better protective performance of the rust layer. The correlation coefficient R^2 obtained from the fitting process reflects the reliability of the model, and when $R^2 > 0.8$, the power-law fitting is considered to be satisfactory and credible for describing the corrosion kinetics.

2.2.6. Electrochemical Tests

Electrochemical tests were carried out using a standard three-electrode system. A 3.5 wt% NaCl solution was used as the electrolyte, and measurements were performed at room temperature using a CS310H electrochemical workstation (WuHan Corrtest Instruments Corp., Ltd., Wuhan, China). The working electrode was the specimen under investigation with an exposed area of 0.785 cm^2, the reference electrode was a saturated calomel electrode (SCE), and a platinum electrode served as the counter electrode. The testing procedure included the following steps: (1) open-circuit potential (OCP) monitoring until the system reached a stable state; (2) electrochemical impedance spectroscopy (EIS) measurement over a frequency range of 10^{-2} to 10^5 Hz; and (3) potentiodynamic polarization scanning within a potential range of ±0.5 V relative to the OCP at a scan rate of 0.5 mV/s. All tests were conducted under a constant temperature of 25 ± 1 °C.

3. Results

3.1. Neutral Salt Spray Corrosion Behavior

3.1.1. Macroscopic Corrosion Morphology

Figure 1 shows the macroscopic morphology evolution of 7075 aluminum alloy during the neutral salt spray test. As the test duration increased, severe corrosion occurred as early as 96 h, with a large amount of white corrosion products forming on the surface. The corrosion product layer appeared porous and loosely structured, with numerous fine pits visible. As the exposure time further increased, both the number and the prominence of these surface pits grew significantly. These observations clearly indicate that 7075 aluminum alloy exhibits poor corrosion resistance under neutral salt spray test conditions.

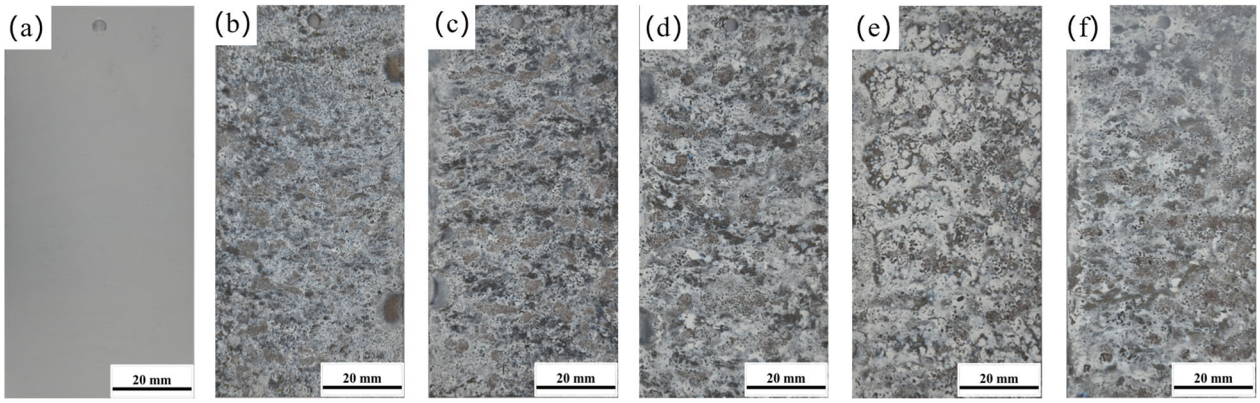


Figure 1. Macroscopic surface morphology of 7075 aluminum alloy after different exposure times in the neutral salt spray test (**a**) 0 h; (**b**) 96 h; (**c**) 240 h; (**d**) 480 h; (**e**) 960 h; (**f**) 1008 h.

3.1.2. Corrosion Product Analysis

Figure 2 shows the microscopic corrosion morphology of 7075 aluminum alloy after different exposure durations in the neutral salt spray test. At the initial stage (96 h, Figure 2a), the corrosion products on the aluminum alloy surface appeared as clustered agglomerates. After removing the corrosion products, visible pits were observed on the surface, which exhibited an uneven texture with pronounced variations in pit depth and size.

During the continued corrosion process from 240 h to 480 h (Figure 2b,c), the initially clustered corrosion products gradually coalesced into block-like formations, resulting in an increased surface coverage by the corrosion products and a significant variation in their height. After removing the surface layer, large-sized corrosion pits were revealed, with the maximum pit depth reaching up to 63.462 μm.

At 720 h (Figure 2d), the corrosion products once again showed a clustered distribution, which is presumed to result from the spallation and subsequent reformation of the surface corrosion product layer. By 1008 h, the corrosion products had almost completely interconnected, forming a continuous surface film.

Table 2 shows the Energy-dispersive spectroscopy (EDS) results for the sample. Analysis indicates that the corrosion products were mainly aluminum oxides composed primarily of Al and O elements, while trace amounts of Na and Cl were also detected, originating from the solidified salt particles deposited on the surface during the salt spray exposure.

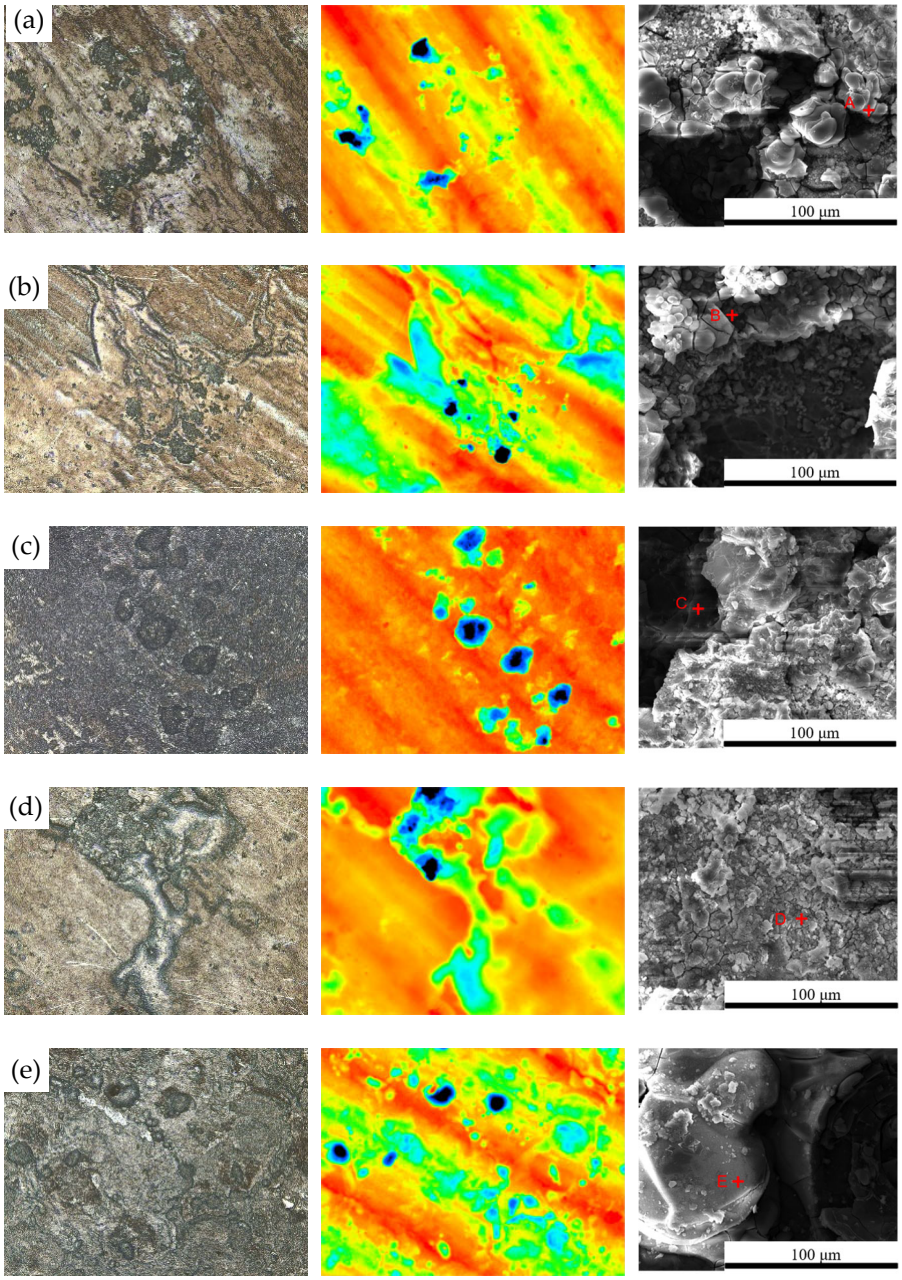


Figure 2. Microscopic surface morphology of 7075 aluminum alloy after different exposure durations in the neutral salt spray test: (**a**) 96 h; (**b**) 240 h; (**c**) 480 h; (**d**) 720 h; (**e**) 1008 h. (Points A, B, C, D and E in the figure represent the EDS energy-dispersive spectroscopy testing points for specimens of different durations).

Table 2. Elemental composition (wt%) of point-scan regions corresponding to Figure 2.

Element	Al	O	Mg	Na	Cu	Cl	Zn
A	64.14	34.16	-	1.70	-	-	-
B	69.21	18.76	3.47	1.66	4.04	2.86	-
C	55.66	33.69	-	-	-	-	10.64
D	60.86	37.45	-	1.68	-	-	-
E	62.88	32.54	4.58	-	-	-	-

Figure 3 shows the cross-sectional morphology of 7075 aluminum alloy after 1008 h of exposure in the neutral salt spray test. The alloy exhibited a relatively thick and irregular

corrosion product layer, with noticeable cracking observed at the interface between the product layer and the substrate.

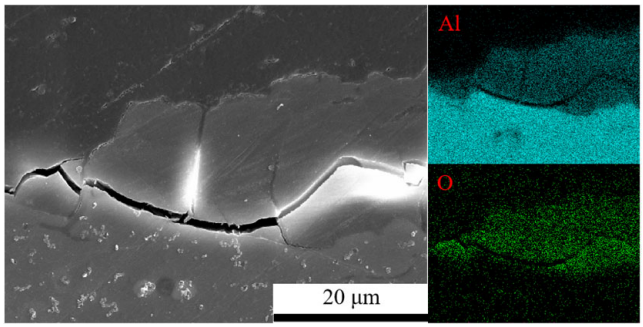


Figure 3. Cross-sectional morphology and elemental distribution of corrosion products on 7075 aluminium alloy under neutral salt spray conditions.

Figure 4 presents the XRD analysis results of 7075 aluminum alloy after 1008 h in the neutral salt spray test. The corrosion products were mainly identified as Al_2O_3 and $Al(OH)_3$.

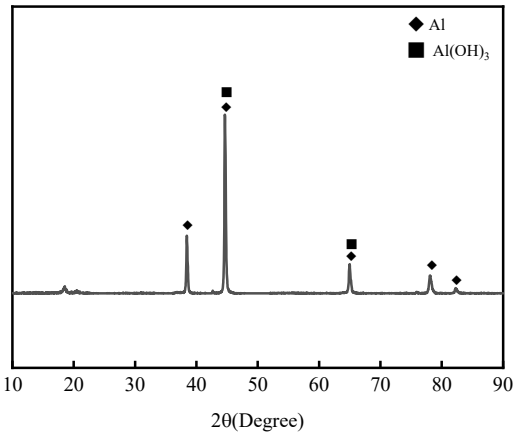


Figure 4. XRD patterns of 7075 aluminum alloy after the neutral salt spray test.

3.1.3. Electrochemical Corrosion Analysis

Figure 5 shows the polarization curves and Tafel fitting results of 7075 aluminum alloy after different exposure times in the neutral salt spray test. As the exposure time increased, variations in the polarization curves reflected different corrosion stages, including passive film breakdown and pitting initiation. The trend of corrosion current density obtained from Tafel extrapolation (Figure 5b) indicates that during the initial stage (0–240 h), the corrosion current remained relatively stable, likely due to the protective effect of the passive film on the aluminum alloy surface. As the exposure time reached 480 h, the corrosion current increased sharply, suggesting the onset of generalized corrosion. At 720 h, the corrosion current decreased significantly, which can be attributed to the full coverage of the alloy surface by the corrosion product layer, providing a temporary barrier effect. In the later stage (1008 h), the corrosion current increased again, possibly due to the spallation of the porous corrosion product layer, which exposed fresh metal to the corrosive environment.

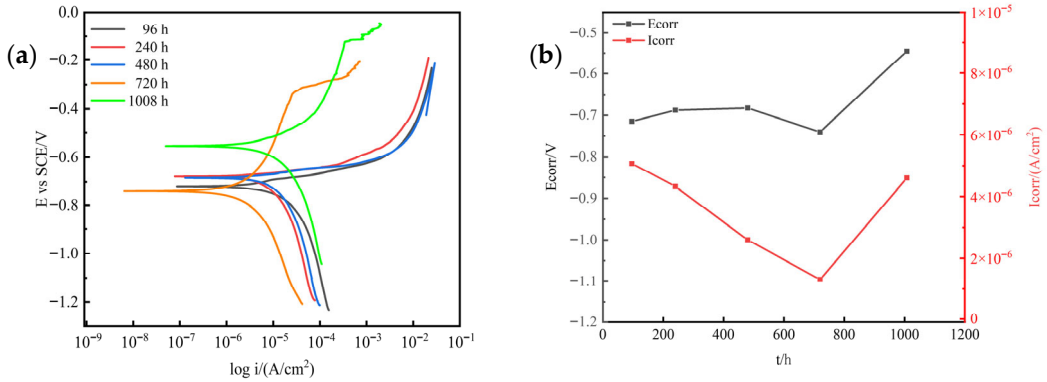


Figure 5. Variation in electrochemical polarization behavior of 7075 aluminum alloy with exposure time in the neutral salt spray test: (**a**) Potentiodynamic polarization curves; (**b**) Corrosion current density and corrosion potential obtained from Tafel fitting.

The negative shift in corrosion potential generally indicates an enhancement of active dissolution. The observed potential variation suggests that during the early stage (0–240 h), the potential change corresponded to the gradual breakdown of the passive film; during 480–720 h, the sharp drop in corrosion potential was associated with the initiation of localized corrosion; and in the later stage (1008 h), the potential fluctuations reflected the alternating processes of corrosion product layer detachment and regeneration.

Therefore, the synchronized variations in corrosion current and potential suggest that in the later stages of exposure, the instability of the corrosion product layer plays a dominant role in controlling the electrochemical response and overall corrosion behavior of 7075 aluminum alloy.

3.2. Correlation Analysis Between Indoor and Outdoor Corrosion Tests

3.2.1. Correlation Analysis of Corrosion Products

Figure 6 shows the macroscopic surface morphology of 7075 aluminum alloy after different exposure durations in the outdoor atmospheric corrosion test conducted in the coastal environment of Hainan. After 6 months of exposure, the surface of the 7075 aluminum alloy lost its metallic luster, and numerous visible white pitting corrosion products appeared. After 12 months, severe corrosion occurred, with a large amount of white corrosion products covering the surface; the corrosion product layer exhibited a loose and porous structure. After 21 months of exposure, the specimens underwent extensive corrosion, and the surface was almost completely covered by corrosion products.

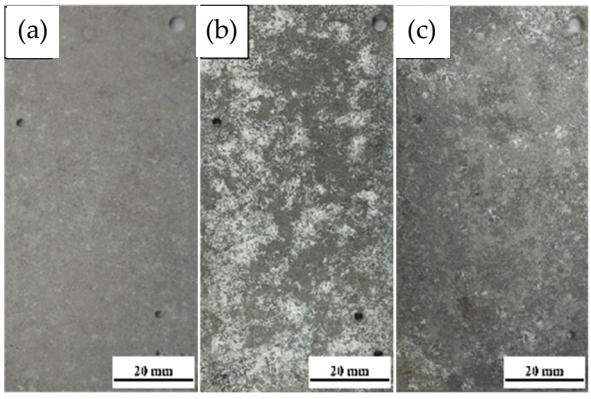


Figure 6. Comparative analysis of macroscopic surface morphology of 7075 aluminum alloy after different exposure durations in the coastal atmospheric environment of Hainan (**a**) 6 months; (**b**) 12 months; (**c**) 21 months.

Figure 7 shows the surface morphology evolution of 7075 aluminum alloy after different exposure durations in the coastal atmospheric environment. After 6 months of exposure, the specimen surface was no longer completely smooth, exhibiting numerous large but shallow corrosion pits distributed across the surface. As the exposure time increased, the surface roughness became more pronounced, with corrosion pits becoming larger, deeper, and more numerous. After 21 months, the maximum pit depth reached 42.51 μm. SEM observations in Figure 7 indicate that the surface corrosion products of 7075 aluminum alloy did not undergo significant compositional or structural changes over time. From 6 months onward, the surface accumulated blocky corrosion products, and as shown in Table 3, the surface oxygen content remained at a consistently high level throughout the exposure period. Combined with the cross-sectional elemental analysis results in Figure 8 for the specimen after 21 months of exposure, a relatively thick corrosion product layer was formed on the surface. The oxygen distribution revealed that the oxide layer was relatively loose and uneven in thickness, with some areas even showing exposed substrate. This may be attributed either to the nonuniform distribution of corrosion initiation sites or to partial detachment of the corrosion product layer.

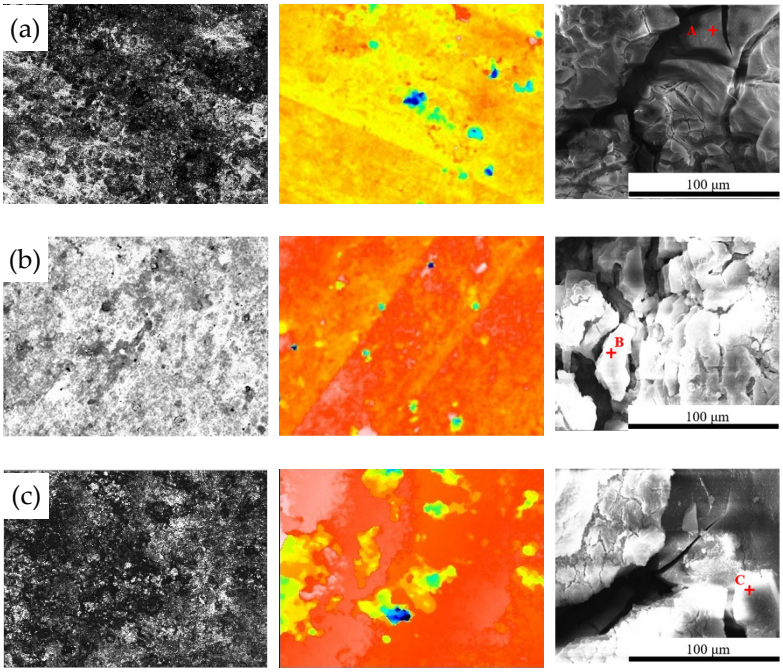


Figure 7. Microscopic structural features of 7075 aluminum alloy after different exposure periods in the coastal atmospheric environment of Hainan: (**a**) 6 months; (**b**) 12 months; (**c**) 21 months. (Points A, B, and C in the figure represent the EDS energy-dispersive spectroscopy testing points for specimens of different durations.).

Table 3. Elemental composition (wt%) of point-scan regions corresponding to Figure 7.

Component	Al	O	Mg
A	49.01	49.20	1.79
B	38.30	61.70	-
C	40.30	59.70	-

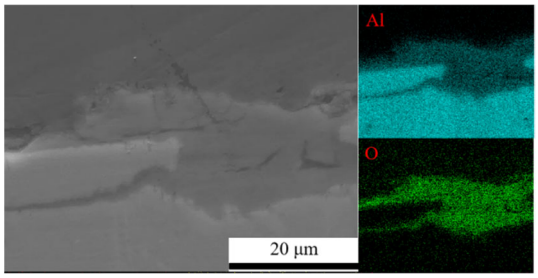


Figure 8. Cross-sectional morphology and elemental distribution of the corrosion product layer on 7075 aluminum alloy.

Figure 9 shows the XRD analysis results of 7075 aluminum alloy after 21 months of outdoor exposure in the coastal atmospheric environment of Hainan. The main corrosion products were identified as $Al(OH)_3$ and Al_2O_3, which are consistent with the results obtained from the indoor neutral salt spray test.

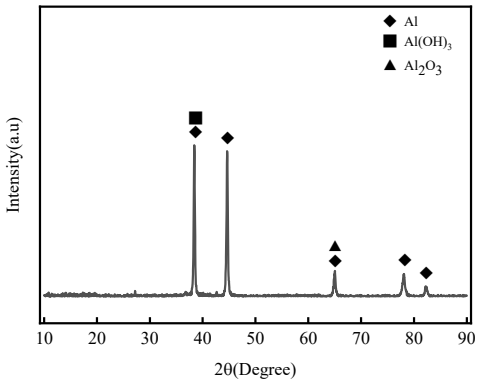


Figure 9. XRD patterns of 7075 aluminum alloy after 21 months of exposure in the coastal atmospheric environment of Hainan.

The main corrosion products of 7075 aluminum alloy in this study—$Al(OH)_3$ and Al_2O_3—are consistent with the phase composition reported in prior research on 7xxx series alloys under marine atmospheric environments. For example, Zhao et al. [14] observed that 7A85 aluminum alloy (a 7xxx variant) formed Al_2O_3 and $Al(OH)_3$ as dominant corrosion products after long-term exposure to industrial-marine atmospheres. Cui et al. [15] also confirmed similar phase compositions in 7A04 alloy exposed to the Xisha tropical marine atmosphere. However, distinct differences exist in the microstructure and stability of the corrosion product layer.

3.2.2. Correlation Analysis of Electrochemical Corrosion Mechanisms

Figure 10 shows the polarization curves and Tafel fitting results of 7075 aluminum alloy after different exposure durations in the outdoor atmospheric corrosion test conducted in the coastal environment of Hainan. As the exposure time increased, the corrosion potential (E_corr) gradually shifted in the positive direction, indicating a decreased tendency toward corrosion. The corrosion current density (I_corr) initially decreased and then increased, suggesting that during the early stage of exposure, a dense corrosion product film formed on the alloy surface, providing temporary protection. However, in the later stage, both corrosion potential and corrosion current increased simultaneously, implying that while the surface corrosion product film remained largely intact, localized selective dissolution occurred at active sites, leading to the exposure of fresh metal and localized corrosion initiation.

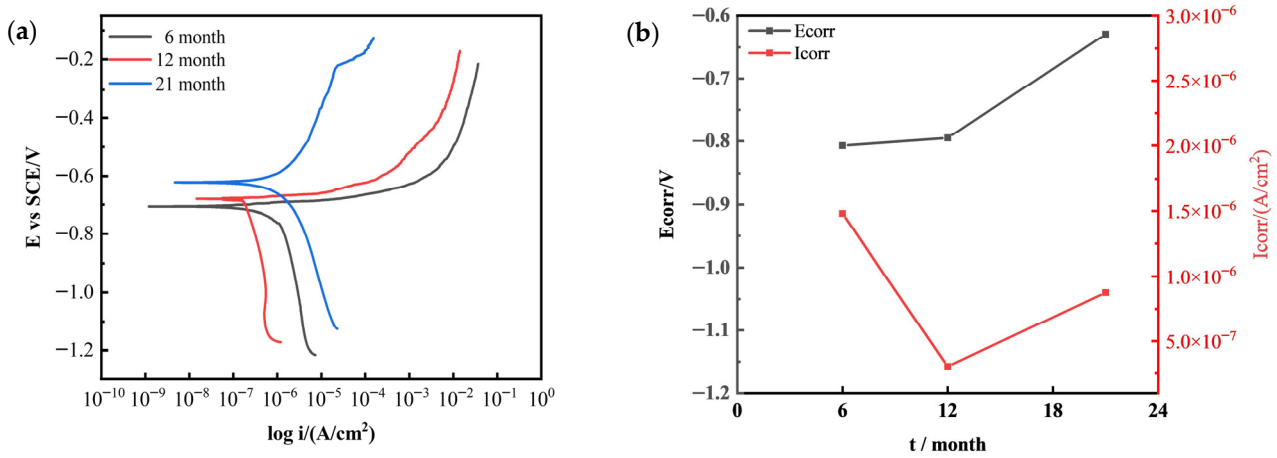


Figure 10. Variation in electrochemical polarization behavior of 7075 aluminum alloy with outdoor exposure time in Hainan: (**a**) Potentiodynamic polarization curves; (**b**) Corrosion current density and corrosion potential obtained from Tafel fitting.

The core reason for the renewed increase in corrosion current in 7075 aluminum alloy during the later stages of both neutral salt spray testing and outdoor exposure to Hainan's marine atmosphere is the detachment of the corrosion product layer. In both test environments, the corrosion products comprised loose, porous $Al(OH)_3$ and Al_2O_3, exhibiting poor structural integrity and weak adhesion to the substrate, providing only temporary protection. Later stages witnessed internal stresses arising from the hydration and expansion of corrosion products, coupled with dynamic environmental influences [15,26]. This led to cracking and detachment at the product-substrate interface, directly exposing fresh alloy substrate. Without passivation film protection, the exposed substrate underwent vigorous anodic dissolution under Cl^- action. Concurrently, the proliferation of active corrosion sites increased electron transfer rates, ultimately causing the corrosion current to rebound [6].

The flaking of aluminum alloy corrosion products primarily occurs when internal stresses generated during the formation of the corrosion layer exceed the interfacial bonding strength with the substrate, triggering delamination [31]. Concurrently, the flaking process is influenced by external environmental factors, particularly moisture-dry cycles and the penetration of corrosive agents such as chloride ions [32]. Following the detachment of corrosion products, the exposed substrate reacts with oxygen and water to form an aluminum oxide passivation layer, initially halting further corrosion. However, this film is unstable in chloride-containing environments, readily breaking down to form soluble $AlCl_3$. The dissolved Al^{3+} ions diffuse outward and hydrolyze to produce $Al(OH)_3$ precipitates, which gradually accumulate to form a new layer of corrosion products.

3.3. Corrosion Mechanism of 7075 Aluminum Alloy Under Chloride Ion Influence in Marine Atmospheric Environments

The high strength of 7075 aluminum alloy primarily originates from nanoscale, age-hardened strengthening precipitates such as $MgZn_2$ (η phase) and Al_2CuMg (S phase). However, these precipitates are anodic relative to the aluminum matrix (α-Al), forming micro-galvanic cells that act as preferential corrosion initiation sites. This micro-galvanic coupling is the fundamental reason for the corrosion susceptibility of 7075 aluminum alloy.

The marine atmospheric environment is characterized by a thin electrolyte film, where high humidity provides the necessary conditions for electrochemical corrosion. The presence of sea-salt particles (e.g., NaCl, $MgCl_2$) is the most critical factor in disrupting the protective alumina (Al_2O_3) passive film. The process is illustrated in Figure 11. Diurnal and

weather-induced fluctuations in temperature and humidity lead to continuous variations in the thickness and concentration of the surface electrolyte film, strongly influencing the corrosion rate and morphology of 7075 aluminum alloy.

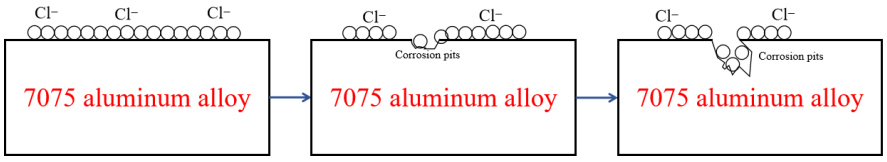


Figure 11. Schematic Diagram of Aluminum Alloy Corrosion Mechanism.

Therefore, the corrosion of 7075 aluminum alloy in a marine atmosphere is a complex, multi-stage process that typically begins with pitting initiation, progresses to intergranular corrosion, and may eventually develop into exfoliation corrosion and stress corrosion cracking. The main driving forces are the breakdown of the passive film by chloride ions and the galvanic effect between the anodic secondary phases (especially $MgZn_2$) and the surrounding matrix. The existence of precipitate-free zones (PFZs) and continuous grain boundary precipitates provides preferential pathways for corrosion propagation.

In the marine atmospheric environment, the corrosion evolution of 7075 aluminum alloy—from initiation and propagation to final structural degradation—can be divided into three main stages:

Stage I: Corrosion initiation—pitting corrosion

Chloride ions (Cl^-) in the marine atmosphere penetrate and locally disrupt the surface alumina (Al_2O_3) passive film of 7075 aluminum alloy. Once the passive film is breached, micro-galvanic couples form between the anodic η phase ($MgZn_2$) and the cathodic aluminum matrix, initiating localized dissolution.

Anodic reaction (occurring at the anodic secondary phase, dissolution of η phase):

$$Zn \rightarrow Zn^{2+} + 2e^- \text{ and } Mg \rightarrow Mg^{2+} + 2e^-$$

Cathodic reaction (occurring on the highly conductive aluminum matrix):

$$O_2 + 2H_2O + 4e^- \rightarrow 4OH^-$$

The preferential dissolution of the anodic phase leads to the formation and growth of corrosion pits. Inside the pits, hydrolysis reactions cause local acidification (a drop in pH), which further accelerates metal dissolution, forming a self-catalyzing vicious cycle.

Stage II: Corrosion propagation—intergranular corrosion

During the aging heat treatment of 7075 aluminum alloy, the continuous distribution of anodic η phases along the grain boundaries and the existence of precipitate-free zones (PFZs) provide rapid pathways for corrosion. In the corrosive medium, chloride ions (Cl^-) penetrate along the grain boundaries, causing selective dissolution of both PFZs and grain-boundary η phases, which form an interconnected corrosion network. The corrosion initiates at the surface and propagates inward along the grain boundaries, while the interior of the grains remains relatively less corroded.

Stage III: Structural failure—exfoliation and stress corrosion cracking (SCC)

Due to rolling or extrusion processes, the grains of 7075 aluminum alloy are typically elongated or flattened. Corrosion propagates laterally along the grain boundaries parallel to the surface. The volumetric expansion of corrosion products lifts the uncorroded surface layers, resulting in lamellar exfoliation. Under tensile stress in actual service conditions, these intergranular corrosion paths can act as crack initiation sites. Crack tips, subjected to high stress concentration and acidic environments, propagate rapidly, leading to brittle

fracture of 7075 aluminum alloy at stresses far below its yield strength. Therefore, stress corrosion cracking is closely associated with intergranular corrosion.

The corrosion behavior in marine atmospheric exposure and neutral salt spray tests differs due to variations in Cl^- concentration, wet/dry cycling, and environmental stability.

In marine atmospheric exposure, alternating wet-dry cycles cause Cl^- to concentrate at oxide film defects as the electrolyte film evaporates, leading to passive film breakdown and pitting initiation. During subsequent wet periods, hydrolysis inside pits promotes acidification and metal dissolution. The following dry periods can cause corrosion products to accumulate at the pit openings, hindering diffusion and intensifying the self-catalytic acidification process within the pits. This intermittent yet cumulative process results in gradual and selective propagation. Because the Cl^- concentration is relatively low, its penetration and selective dissolution along the grain-boundary anodic regions (η phase and PFZ) occur more preferentially and distinctly, forming typical intergranular corrosion morphologies that progress slowly and steadily inward.

In contrast, neutral salt spray tests maintain a continuous, high-concentration Cl^- environment that persistently attacks the oxide film of 7xxx series aluminum alloys. Although this condition can rapidly initiate pitting, the entire surface is immersed in a highly conductive electrolyte, favoring widespread surface corrosion rather than selective propagation along specific grain boundaries. The intense general corrosion and accumulation of corrosion products may obscure or mask distinct intergranular features. At the microscopic level, intergranular corrosion may still occur, but its contrast and definition are reduced due to the predominance of uniform surface attack.

3.4. Kinetic Prediction Model for 7075 Aluminum Alloy Under Neutral Salt Spray Acceleration

The native alumina (Al_2O_3) film on the surface of 7075 aluminum alloy serves as its only natural corrosion barrier. In both marine atmospheric exposure and neutral salt spray environments, chloride ions (Cl^-), owing to their small ionic radius, strong penetrability, and high surface adsorption capability, can competitively adsorb onto the oxide film, particularly at defects, dislocations, and grain boundaries. Cl^- reacts with alumina to form soluble $AlCl_3$ or chloro-oxy complexes; however, these compounds are typically unstable and undergo hydrolysis, leading to localized dissolution and breakdown of the oxide film and the exposure of the active aluminum substrate.

Consequently, since Cl^- concentration and wet–dry cycling varies between marine atmospheric exposure and neutral salt spray tests, the corrosion kinetics of 7075 aluminum alloy also differ. As shown in Figure 11, the corrosion mass loss of 7075 aluminum alloy increases significantly with time under neutral salt spray conditions, while the rate of mass loss gradually decreases. Both the rate of increase in mass loss and the rate of decrease in corrosion rate slow over time, indicating that the corrosion rate declines progressively as exposure continues. This behavior demonstrates that the corrosion products formed during testing provide a certain degree of protection to the underlying alloy substrate.

Figure 12 shows the corrosion mass loss and mass loss rate of 7075 aluminium alloy specimens at different exposure durations during neutral salt spray testing. By fitting the mass-loss data of 7075 aluminum alloy using the nonlinear power-law Equation (3), an excellent correlation coefficient ($R^2 = 0.99268$) was obtained, confirming that the corrosion kinetics follow a power-law relationship. The derived kinetic model for 7075 aluminum alloy in the neutral salt spray test is expressed as:

$$\Delta W = 1.323t^{0.454} \quad (4)$$

where ΔW is the corrosion mass loss per unit area ($g \cdot m^{-2}$), and t is the exposure time (h). This model quantitatively describes the time-dependent corrosion behavior of 7075 aluminum alloy under neutral salt spray acceleration conditions.

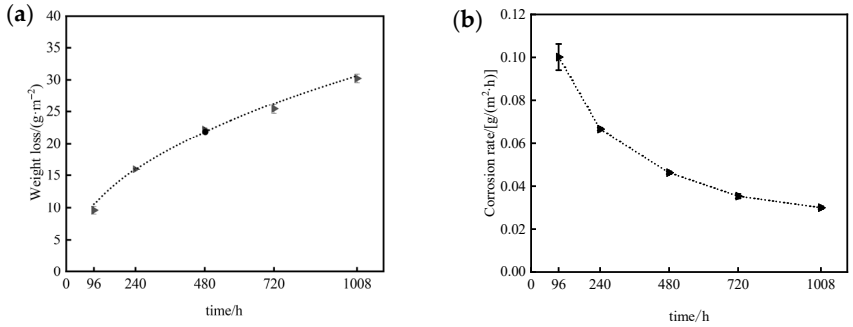


Figure 12. Corrosion mass loss and mass loss rate of 7075 aluminum alloy after different exposure durations in the neutral salt spray test: (**a**) Corrosion mass loss; (**b**) Corrosion mass loss rate.

Based on the weight loss measurements of 7075 aluminum alloy specimens exposed for 6, 12 and 21 months in the coastal atmospheric environment of Hainan (Table 4), it was found that the acceleration factor calculated using the neutral salt spray kinetic model (Equation (4)) decreased from approximately 45.1× at 6 months to about 26.8× at 21 months. This finding indicates that the high Cl^- concentration in the neutral salt spray test significantly accelerates the corrosion of 7075 aluminum alloy, while the rapid formation of corrosion products subsequently slows down the corrosion process.

Table 4. Corrosion mass loss of 7075 aluminum alloy after 21 months of exposure in the coastal atmospheric environment of Hainan.

Outdoor Exposure Time (Months)	Corrosion Mass Loss (g/m^2)	Corresponding Neutral Salt Spray Time (h)	Corrosion Rate ($g/m^2 \cdot h$)	Acceleration Factor
6	11.01	194.65	0.07449	45.1
12	14.50	502.33	0.04435	34.9
21	20.50	1305.03	0.02625	26.8

During the 21-month outdoor exposure in the Hainan coastal atmosphere, the protective effect of the corrosion product layer also led to a nonlinear power-law relationship between corrosion mass loss and time, where the corrosion rate gradually decreased with increasing exposure duration. By applying Equation (3) and using the one-year outdoor exposure weight loss as the reference, the constants were determined as $A = 4.19933$ and $n = 0.51641$. Thus, the corrosion kinetics model of 7075 aluminum alloy under the Hainan coastal atmospheric environment can be expressed as:

$$\Delta W = 4.19933 t^{0.51641} \quad (5)$$

This model demonstrates that the corrosion of 7075 aluminum alloy in the marine atmosphere follows a similar nonlinear kinetic trend to that observed in the neutral salt spray test but progresses at a slower rate due to the lower Cl^- concentration and the stabilizing influence of the corrosion product layer formed under natural environmental conditions.

Therefore, by integrating both corrosion kinetics and electrochemical analyses, a quantitative relationship can be established between the corrosion rates of 7075 aluminum alloy under indoor and outdoor environments. The fitting results are shown in Figure 13. Com-

bining Equations (4) and (5), the corresponding acceleration factors between the Hainan coastal atmospheric exposure and the neutral salt spray test were calculated. However, due to the inherent complexity of the real marine atmospheric environment, which involves variable temperature, humidity, salt deposition, and cyclic wet–dry conditions not replicated in the salt spray test, the relationship between the two environments cannot be expressed as a simple linear function. By fitting the acceleration factor data between the indoor and outdoor tests using the power-law Equation (3), the fitting constants were determined as A = 93.75222 and n = −0.40558. Thus, the model describing the acceleration factor (y) of the neutral salt spray test relative to the outdoor atmospheric exposure can be expressed as:

$$y = 93.75222t^{-0.40558} \quad (6)$$

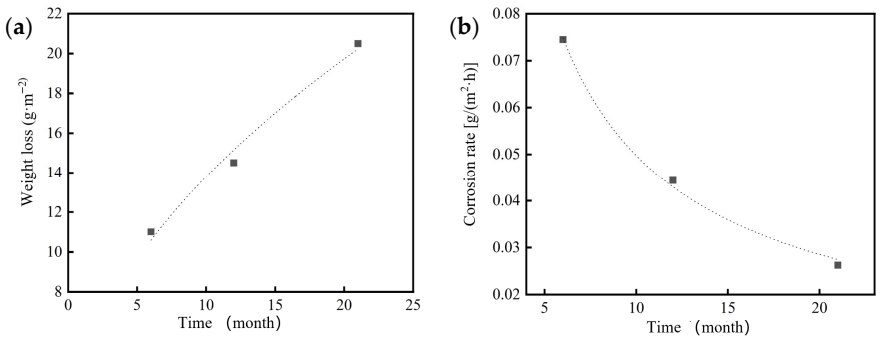


Figure 13. Corrosion mass loss and mass loss rate of 7075 aluminum alloy after different exposure durations in the coastal atmospheric environment of Hainan: (**a**) Corrosion mass loss; (**b**) Corrosion mass loss rate.

This model indicates that the acceleration factor gradually decreases with increasing exposure time, reflecting the transition from an initially aggressive corrosion stage to a relatively stabilized stage dominated by the protective effect of the corrosion product layer.

As shown in Figure 14, the correlation and acceleration factor relationship between the neutral salt spray test and the marine atmospheric environment indicate that the neutral salt spray test serves as an effective and rapid comparative method for quality control and material screening. However, as the test duration increases, the acceleration factor relative to the marine atmospheric environment gradually decreases and eventually stabilizes. This suggests that for 7xxx series aluminum alloys—materials that are highly sensitive to localized corrosion, especially intergranular corrosion and stress corrosion cracking—short-term neutral salt spray tests may yield acceleration factors that can be misleading when extrapolated to real marine exposure conditions.

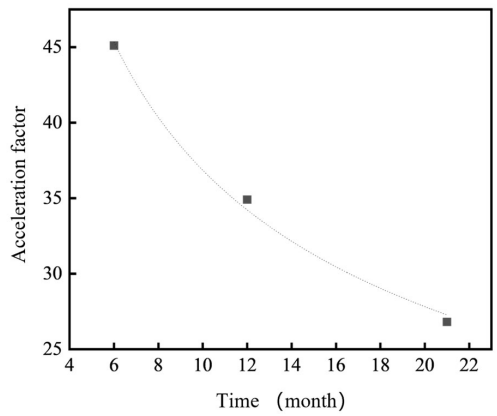


Figure 14. Correlation and acceleration factor relationship between neutral salt spray test and outdoor atmospheric exposure.

4. Conclusions

7075 aluminum alloy exhibited poor corrosion resistance in the neutral salt spray test, showing severe corrosion after only 96 h. The corrosion products were loose, white, cluster-like structures. Although the thickening of the corrosion product layer slowed the corrosion process, its protective ability was limited; subsequent spallation caused potential fluctuations, confirming that the stability of the product layer is crucial for effective protection.

The corrosion weight loss of 7075 aluminum alloy in the neutral salt spray test followed a power-law relationship, with a rapid initial corrosion rate that slowed over time due to the protective effect of the corrosion product layer. The outdoor exposure test in the Hainan coastal atmosphere showed a similar trend, but the actual corrosion rate was influenced by environmental complexity. Under equivalent corrosion levels, the acceleration factor of the neutral salt spray test decreased with prolonged exposure, indicating that the protective behavior of corrosion products in real environments is dynamically regulated by multiple factors.

The corrosion products in both the neutral salt spray test and the Hainan coastalatmospheric environment were mainly composed of $Al(OH)_3$ and Al_2O_3, and the microstructures exhibited characteristic pits and porous corrosion product layers. Electrochemical analyses in both environments showed that the corrosion current–potential relationship was dominated by the stability of the corrosion product layer, demonstrating consistent underlying mechanisms.

Due to the complex environmental factors in the Hainan coastal atmosphere—including humidity, temperature, and chloride deposition—the neutral salt spray test can effectively simulate chloride-induced corrosion mechanisms but cannot fully reproduce the coupled effects of natural environmental conditions. Therefore, its kinetic model cannot be directly extrapolated to real-world corrosion behavior using a simple acceleration factor. When evaluating marine environmental adaptability, the salt spray test results should not be directly equated with actual service performance.

Author Contributions: Conceptualization, C.C. and K.X.; methodology, X.M.; software, Z.S.; validation, C.C., X.M. and K.X.; formal analysis, Z.S.; investigation, C.C.; resources, C.C.; data curation, K.X.; writing—original draft preparation, C.C. and K.X.; writing—review and editing, C.C.; visualization, K.X.; supervision, C.C.; project administration, C.C.; funding acquisition, C.C. All authors have read and agreed to the published version of the manuscript.

Funding: This research received no external funding.

Data Availability Statement: The original contributions presented in this study are included in the article. Further inquiries can be directed to the corresponding author.

Acknowledgments: The authors acknowledge the platform support of the National Material Corrosion and Protection Science Data Center.

Conflicts of Interest: The authors declare no conflicts of interest.

References

1. Babu, K.A.; Venkataramaiah, P.; Yerrathota, S. Material selection for preparation of aluminium hybrid Mmcs. *Mater. Today Proc.* **2018**, *5*, 12209–12222. [CrossRef]
2. Koprowski, P.; Lech-Grega, M.; Wodziński, Ł.; Augustyn, B.; Boczkal, S.; Ożóg, M.; Uliasz, P.; Żelechowski, J.; Szymański, W. The effect of low content additives on strength, resistivity and microstructural changes in wire drawing of 1xxx series aluminium alloys for electrical purposes. *Mater. Today Commun.* **2020**, *24*, 101039. [CrossRef]
3. Zhou, B.; Liu, B.; Zhang, S. The advancement of 7xxx series aluminum alloys for aircraft structures: A review. *Metals* **2021**, *11*, 718. [CrossRef]

4. Zhong, X.; Liu, J.; Liu, Y.; Fan, J.; Pu, J. Enhanced repassivation accelerates wear: Tribocorrosion mechanism of 7075 Al Alloy in marine atmosphere environment. *Tribol. Int.* **2025**, *215*, 111502. [CrossRef]
5. Czerwinski, F. Aluminum alloys for electrical engineering: A review. *J. Mater. Sci.* **2024**, *59*, 14847–14892. [CrossRef]
6. Xiang, L.; Tao, J.; Xia, X.; Zhao, Z.; Chen, Q.; Su, Y.; Chai, S.; Zheng, Z.; Sun, J. Impact of Marine Atmospheric Corrosion on the Microstructure and Tensile Properties of 7075 High-Strength Aluminum Alloy. *Materials* **2023**, *16*, 2396. [CrossRef] [PubMed]
7. Ezuber, H.; El-Houd, A.; El-Shawesh, F. A study on the corrosion behavior of aluminum alloys in seawater. *Mater. Des.* **2008**, *29*, 801–805. [CrossRef]
8. Zhu, H.; Liu, W.; Su, H.; Wang, X.; Yao, X. Corrosion Behavior of 2A14 Aluminum Alloy under Marine Atmospheric Corrosion Conditions. *J. Mater. Eng. Perform.* **2025**, 1–13. [CrossRef]
9. Zhang, T.; Wu, S.; Liu, H.; Yang, L.; Chen, T.; Wang, X.; Li, Y. Research on Comparative Marine Atmospheric Corrosion Behavior of AZ31 Magnesium Alloy in South China Sea. *Materials* **2025**, *18*, 3585. [CrossRef]
10. Shi, B.; Wang, L.; Qin, L.; Guo, X.; Yang, G.; Wu, W.; Li, Z.; Cheng, X. Corrosion behavior of aluminum alloys in harsh marine atmospheric environment. *Anti-Corros. Methods Mater.* **2025**, *72*, 761–775. [CrossRef]
11. Shi, B.; Wang, L.; Cheng, X.; He, Z.; Qin, L.; Guo, X.; Wang, H.; Li, Z.; Li, X. Study the impact of secondary phases on the corrosion resistance and mechanical properties of aluminum alloys under simulated harsh marine environment. *Surf. Interfaces* **2025**, *59*, 105994. [CrossRef]
12. Yang, Y.; Kim, S. Electrochemical Characteristics of Aluminum Alloys in Sea Water for Marine Environment. *Acta Phys. Pol. A* **2019**, *135*, 1005–1011. [CrossRef]
13. Fu, Y.; Mehr, V.Y.; Toroghinejad, M.R.; Chen, X.; Jie, J.; Zhu, S. Twinning and stacking fault-induced precipitation in an aluminum alloy. *J. Mater. Res. Technol.* **2025**, *34*, 2127–2132. [CrossRef]
14. Zhao, Q.; Guo, C.; Niu, K.; Zhao, J.; Huang, Y.; Li, X. Long-term corrosion behavior of the 7A85 aluminum alloy in an industrial-marine atmospheric environment. *J. Mater. Res. Technol.* **2021**, *12*, 1350–1359. [CrossRef]
15. Cui, Z.Y.; Li, X.G.; Man, C.; Xiao, K.; Dong, C.F.; Wang, X.; Liu, Z.Y. Corrosion behavior of field-exposed 7A04 aluminum alloy in the Xisha tropical marine atmosphere. *J. Mater. Eng. Perform.* **2015**, *24*, 2885–2897. [CrossRef]
16. Cai, B.; Xu, Z.; Liu, G.; Li, Y.; Yan, L.; Pang, X.; Gao, K. Understanding of the occurrence of intergranular corrosion in 2024 aluminum alloy under atmospheric environment. *J. Mater. Res. Technol.* **2025**, *35*, 6690–6699. [CrossRef]
17. Wahid, M.A.; Siddiquee, A.N.; Khan, Z.A. Aluminum alloys in marine construction: Characteristics, application, and problems from a fabrication viewpoint. *Mar. Syst. Ocean Technol.* **2020**, *15*, 70–80. [CrossRef]
18. Jebaraj, A.V.; Aditya, K.; Kumar, T.S.; Ajaykumar, L.; Deepak, C. Mechanical and corrosion behaviour of aluminum alloy 5083 and its weldment for marine applications. *Mater. Today Proc.* **2020**, *22*, 1470–1478. [CrossRef]
19. Shamsudeen, S.; John, E.R.D. Effect of welding on pitting and intergranular corrosion behavior of marine grade aluminum alloy. *Mater. Perform. Charact.* **2019**, *8*, 555–570. [CrossRef]
20. Cui, Z.Y.; Li, X.G.; Xiao, K.; Dong, C.F.; Wang, L.W.; Zhang, D.W.; Liu, Z.Y. Exfoliation corrosion behavior of 2B06 aluminum alloy in a tropical marine atmosphere. *J. Mater. Eng. Perform.* **2015**, *24*, 296–306. [CrossRef]
21. Wang, L.; Wang, H.; Li, B.; Yu, H.; Zhang, H.; Chen, J.; Yin, C.; Xiao, K. Study on Constructing Indoor Accelerated Simulation Methods for Steel with Galvalume Coating Exposed to Marine Atmosphere. *Metals* **2025**, *15*, 1143. [CrossRef]
22. Kang, W.; Zhang, H.; Chu, C.; Wang, L.; Hu, Y.; Ding, Y.; Zhang, D. Hot corrosion behavior of IN738LC alloy formed by selective laser melting. *Corros. Sci.* **2022**, *198*, 110154. [CrossRef]
23. Peng, J.; Xie, S.; Xia, J.; Wang, X.; Ni, Z.; Wang, P.; Chen, N. Investigation of Process and Properties of Cu-Mn-Al Alloy Cladding Deposited on 27SiMn Steel via Cold Metal Transfer. *Crystals* **2025**, *15*, 858. [CrossRef]
24. Finke, A.; Escobar, J.; Munoz, J.; Petit, M. Prediction of salt spray test results of micro arc oxidation coatings on AA2024 alloys by combination of accelerated electrochemical test and artificial neural network. *Surf. Coatings Technol.* **2021**, *421*, 127370. [CrossRef]
25. Usman, B.; Scenini, F.; Curioni, M. The effect of exposure conditions on performance evaluation of post-treated anodic oxides on an aerospace aluminium alloy: Comparison between salt spray and immersion testing. *Surf. Coat. Technol.* **2020**, *399*, 126157. [CrossRef]
26. Diler, E.; Peltier, F.; Becker, J.; Thierry, D. Real-time corrosion monitoring of aluminium alloys under chloride-contaminated atmospheric conditions. *Mater. Corros.* **2021**, *72*, 1377–1387. [CrossRef]
27. Schindelholz, E.; Kelly, R.G. Wetting phenomena and time of wetness in atmospheric corrosion: A review. *Corros. Rev.* **2012**, *30*, 135–170. [CrossRef]
28. Ramdé, T.; Fedel, M.; Rossi, S. The Effect of Spray Testing Condition on the Corrosion Performance of Hydrothermally Sealed Anodic Oxide on a 5005 Aluminum Alloy: Comparison between Neutral Salt Spray, Acetic Salt Spray and Prohesion Testing Methods. *J. Electrochem. Soc.* **2024**, *171*, 041501. [CrossRef]
29. *GB/T 16545-2015*; Corrosion of Metals and Alloys-Removal of Corrion Products from Corrosion Test Sprcimen. Standardization Administration of China (SAC): Beijing, China, 2015.

30. *GB/T 14165-2008*; Corrosion of Metals and Alloys-Atmospheric Corrosion Test-General Requirements for Field Tests. Standardization Administration of China (SAC): Beijing, China, 2008.
31. Tian, H.; Cui, Z.; Zhang, B.; Yang, W.; Yang, Y.; Cui, H. Atmospheric corrosion and mechanical property degradation of 2524-T3 aluminum alloy in marine environments. *Corros. Sci.* **2024**, *239*, 112398. [CrossRef]
32. Lamloum, C.; Gharbi, O.; Belliard, L.; Vivier, V.; Ngo, K. Real-time monitoring of the uniform corrosion rate of aluminum using picosecond acoustic method. *Measurement* **2025**, *253*, 117696. [CrossRef]

Disclaimer/Publisher's Note: The statements, opinions and data contained in all publications are solely those of the individual author(s) and contributor(s) and not of MDPI and/or the editor(s). MDPI and/or the editor(s) disclaim responsibility for any injury to people or property resulting from any ideas, methods, instructions or products referred to in the content.